Transaction of JASCOME Vol. 22 (Dec., 2022), Paper No. 02-221216 JASCOME

Accuracy Controllable Characteristic Basis Function Method by using Krylov Subspace Algorithm

Tai TANAKA[1,2)], Kazuki NIINO[3)], Naoshi NISHIMURA[4)], and Michio TAKIKAWA[5)]

1) Kyoto University (36-1 Yoshida-Honmachi, Sakyo-ku, Kyoto 606-8501, E-mail: tanaka.tai.76a@st.kyoto-u.ac.jp)
2) Mitsubishi Electric Corp. (2-7-3, Marunouchi, Chiyoda-ku, Tokyo 100-8310, E-mail: Tanaka.Tai@dh.MitsubishiElectric.co.jp)
3) Kyoto University (36-1 Yoshida-Honmachi, Sakyo-ku, Kyoto 606-8501, E-mail: niino@i.kyoto-u.ac.jp)
4) Kyoto University (36-1 Yoshida-Honmachi, Sakyo-ku, Kyoto 606-8501, E-mail: nishimura.naoshi.8r@kyoto-u.jp)
5) Mitsubishi Electric Corp. (2-7-3, Marunouchi, Chiyoda-ku, Tokyo 100-8310, E-mail: Takikawa.Michio@ak.MitsubishiElectric.co.jp)

We propose a hybrid algorithm of the method of moments (MoM) and the characteristic basis function method (CBFM), which can rapidly and accurately calculate angular characteristics of scattered waves for electromagnetic incident waves from multiple directions. The proposed method roughly captures characteristics of a solution by the CBFM, and the accuracy of the solution is further controlled with the help of the Krylov subspace method in the MoM. Also the number of sampling points of the incident plane waves in the computation of generating the CBFs is small. We analyzed the monostatic radar cross section pattern of two scatterers by using the proposed method. The accuracy improvement can be achieved by the hybrid algorithm, which is faster than the conventional MoM.

Key Words : Method of Moments (MoM), Characteristic Basis Function Method (CBFM), Radar Cross Section (RCS).

1. Introduction

Numerical analyses for electromagnetic scattering are studied for various purposes in engineering such as design of wireless communication systems and radar systems. When analyzing scattering properties of a structure, a plane wave is often used as the incident field. In general, the scattering properties depend on the incident angle of the plane wave. The scattered field for each incident field is often evaluated by the radar cross section (RCS), which is the ratio of the norm of a scattered field to that of the incident field [1].

There exist many methods to evaluate RCSs for electromagnetic scattering problems. For example, the high-frequency approximation methods based on uniform diffraction theory [2] and the numerical methods such as the finite element method [3], the finite-difference time-domain method [4], and the method of moments (MoM) [5] are well known as typical methods for the analysis of the electromagnetic problems. Among these methods, the MoM can analyze scattering problems in open regions with very high accuracy. In the MoM, the integral equation are discretized and transformed into a system of linear equations by the Galerkin method. Since the coefficient matrix of that linear equation is dense, it is difficult for a naive MoM to solve large-scale problems. However, it is well known that the fast multipole method (FMM) can compute the product of the dense matrix and arbitrary vectors faster thus providing a fast method of solving large-scale problems along with iterative linear solvers [6, 7].

As another approach for acceleration and reduction of the memory usage in the MoM, the domain decomposition methods have been considered [8, 9]. They can reduce the computational complexity and memory usage by a low-rank approximation of the matrix equations. Among various domain decomposition methods, the characteristic basis function method (CBFM) is known to be effective for problems with multiple sources and finite periodic scatterers such as the array antennas [10–13]. In the CBFM, scatterers are divided into multiple cells and the characteristic basis functions (CBFs) are defined as non-local basis functions in each cell. The CBFs in each cell are obtained as a sub-matrix solution corresponding to elementary basis functions such as the Rao-Wilton-Glisson (RWG) function [14] with multiple incident plane waves. In general, the number of CBFs is much less than that of the RWG functions; hence the computational cost for solving integral equations discretized with the CBFs is smaller than that with the RWG. However, the CBFM has a trade-off between the computational time for generating the CBFs and accuracy of the final solution. Indeed, it takes much computational time for generating the CBFs if the number of incident plane waves is increased while smaller numbers of incident waves for CBF generation leads to poor accuracy. In order to solve this problem, we have proposed a new type of CBF called the improved primary CBF (IPCBF) [15, 16]. This method takes into account the coupling effects between cells (the higher-order CBFs [17]),

received Oct. 4, 2022, accepted Nov. 10, 2022

which are solutions of the submatrix equation with waves radiated from other cells as incident waves. The CBFM using the IPCBFs is particularly useful as a way to roughly check the angular characteristics of the scattered field.

In this paper, we propose a hybrid of the conventional MoM and the CBFM as a method to further improve the accuracy while taking advantages of the IPCBFs. In the proposed method, the characteristics of the solution are roughly identified by CBFM, and the accuracy of the solution is further controlled by the MoM. The proposed method can seamlessly select cases where the accuracy of CBFM is sufficient, thus mitigating the problem related to the trade-off between accuracy and efficiency.

The article consists of the following components. First, we present the preliminary description of the MoM in next section. In section 3, we show detailed expression of the proposed algorithm. In section 4, the validity of the formulation is shown by numerical evaluations. Finally, we show some concluding remarks. We use following symbols in this paper. The bold and italicized symbols such as $\boldsymbol{A}$ represent vector quantities in three-dimensional fields. The uppercase and lowercase symbols $\mathbf{A}$, $\mathbf{a}$ written in bold and upright type represent matrices and vectors, respectively. The expression such as $\left[\mathbf{A}\right]_{ij}$ denotes an element of a matrix or vector. A matrix or vector with a subscript such as $\mathbf{A}_{ij}$, $(\mathbf{A})_{ij}$ is a subset or a subvector, respectively. The matrix with the superscript H represents the adjoint matrix, and $\boldsymbol{A}\cdot\boldsymbol{B}=\sum_i [\bar{A}]_i[B]_i$ is the (complex) inner product of vectors $\boldsymbol{A}$ and $\boldsymbol{B}$. In addition, RCS means monostatic RCS, not bistatic RCS [1].

2. Integral equations and MoM

In this section, we present a preliminary description of the MoM.

2.1. Integral Equation

We assume that domain Ω is a perfect electric conductor, and $D=\mathbb{R}^3\setminus\bar{\Omega}$ is the analysis space as shown in Fig. 1. $\Gamma=\partial\Omega$ is the closed surface of the PEC. The unit normal vector $\hat{\boldsymbol{n}}$ points in the direction of D. Hereinafter we assume the time dependence to be $e^{j\omega t}$ and suppress it. The electric field integral equation (EFIE) and the magnetic field integral equation (MFIE) [18] are represented by

$$\hat{\boldsymbol{n}}\times\hat{\boldsymbol{n}}\times\boldsymbol{E}^{\mathrm{inc}}(\boldsymbol{r})=-\eta\hat{\boldsymbol{n}}\times(\mathcal{T}\boldsymbol{J})(\boldsymbol{r}), \tag{1}$$

$$\hat{\boldsymbol{n}}\times\boldsymbol{H}^{\mathrm{inc}}(\boldsymbol{r})=-(\mathcal{K}\boldsymbol{J})(\boldsymbol{r})+\frac{1}{2}\boldsymbol{J}(\boldsymbol{r}). \tag{2}$$

Here, $\boldsymbol{J}(\boldsymbol{r})$ is the unknown surface current on Γ. The integral

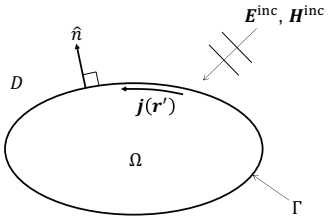

Fig. 1: Definition of the domain

operators $\mathcal{T}$ and $\mathcal{K}$ are defined as

$$\begin{aligned}(\mathcal{T}\boldsymbol{J})(\boldsymbol{r})&=jk\hat{\boldsymbol{n}}\times F.P.\int_\Gamma\left(\mathcal{I}+\frac{1}{k^2}\nabla\nabla\right)G(\boldsymbol{r},\boldsymbol{r}')\boldsymbol{J}(\boldsymbol{r}')d\boldsymbol{r}'\\&\equiv\hat{\boldsymbol{n}}\times(\mathcal{T}'\boldsymbol{J})(\boldsymbol{r})\end{aligned} \tag{3}$$

$$(\mathcal{K}\boldsymbol{J})(\boldsymbol{r})=\hat{\boldsymbol{n}}\times P.V.\int_\Gamma\boldsymbol{J}(\boldsymbol{r}')\times\nabla G(\boldsymbol{r},\boldsymbol{r}')d\boldsymbol{r}' \tag{4}$$

Here, $F.P.$, $P.V.$, and $\mathcal{I}$ represent the finite part, the Cauchy principal value integral, and the identity operator, respectively. Also $\boldsymbol{E}^{\mathrm{inc}}$ and $\boldsymbol{H}^{\mathrm{inc}}$ denote the incident electric and magnetic fields. The wavenumber, impedance of the free space and imaginary unit are denoted by k, η, and j, respectively. The function $G(\boldsymbol{r},\boldsymbol{r}')$ is the fundamental solution of Helmholtz's equation in three-dimension space for the observation point $\boldsymbol{r}$ and the source point $\boldsymbol{r}'$:

$$G(\boldsymbol{r},\boldsymbol{r}')=\frac{e^{-jk|\boldsymbol{r}-\boldsymbol{r}'|}}{4\pi|\boldsymbol{r}-\boldsymbol{r}'|} \tag{5}$$

We have the combined field integral equation (CFIE) in the following form:

$$\begin{aligned}&-\gamma\hat{\boldsymbol{n}}\times\hat{\boldsymbol{n}}\times\boldsymbol{E}^{\mathrm{inc}}(\boldsymbol{r})+(1-\gamma)\eta\hat{\boldsymbol{n}}\times\boldsymbol{H}^{\mathrm{inc}}(\boldsymbol{r})\\&\quad=\gamma\eta\hat{\boldsymbol{n}}\times(\mathcal{T}\boldsymbol{J})(\boldsymbol{r})-(1-\gamma)\eta(\mathcal{K}\boldsymbol{J})(\boldsymbol{r})+\frac{1}{2}(1-\gamma)\eta\boldsymbol{J}(\boldsymbol{r}),\end{aligned} \tag{6}$$

where γ is coefficients of the combination of (1) and (2). We use the CFIE for analyzing the problem in this paper.

2.2. Discretization of Integral Equations

In this analysis, the scatterers are discretized with triangles and RWG basis function [14] $\boldsymbol{f}_n(\boldsymbol{r})$ defined on the triangular mesh. The unknown current $\boldsymbol{J}(\boldsymbol{r})$ is expanded with the RWG function:

$$\boldsymbol{J}(\boldsymbol{r})\approx\sum_{n=1}^{N}\alpha_n\boldsymbol{f}_n(\boldsymbol{r}),\quad\alpha_n\in\mathbb{C} \tag{7}$$

Taking the inner product of RWG basis and the integral equation in (6), we obtain the matrix equation [5]

$$\mathbf{Zj}=\mathbf{v} \tag{8}$$

where $\mathbf{Z}\in\mathbb{C}^{N\times N}$ and $\mathbf{v}\in\mathbb{C}^N$ are respectively the impedance

matrix and incident field vector, which are defined by

$$\left[\mathbf{Z}\right]_{mn} = \int_{\Gamma} \boldsymbol{f}_m(\boldsymbol{r}) \cdot (\gamma\eta\hat{\boldsymbol{n}} \times (\mathcal{T}\boldsymbol{f}_n)(\boldsymbol{r}) - (1-\gamma)\eta\,(\mathcal{K}\boldsymbol{f}_n)(\boldsymbol{r}) + \frac{1}{2}(1-\gamma)\eta\boldsymbol{f}_n(\boldsymbol{r}))d\boldsymbol{r}, \quad (9)$$

$$\left[\mathbf{v}\right]_m = \int_{\Gamma} \boldsymbol{f}_m(\boldsymbol{r}) \cdot (-\gamma\hat{n} \times \hat{n} \times \boldsymbol{E}^{\mathrm{inc}}(\boldsymbol{r}) + (1-\gamma)\eta\hat{n} \times \boldsymbol{H}^{\mathrm{inc}}(\boldsymbol{r}))d\boldsymbol{r}. \quad (10)$$

In the conventional MoM, we solve equation (8) with an iterative method or a direct method to obtain the solution as the expansion coefficient vector $\mathbf{j} = \begin{bmatrix}\alpha_1 & \alpha_2 & \cdots & \alpha_N\end{bmatrix}^T$ where the superposed T stands for the transpose of a vector.

The convergence of (8) is usually good because the discretized MFIE included in the CFIE has a small condition number. Since the condition number of the EFIE is large, the convergence of (8) becomes worse as the coefficient γ of the CFIE is set to larger values. On the other hand, the accuracy of the analysis improves [7].

3. Formulation of Proposed Method

3.1. Overview of CBFM

The CBFM is a numerical method to accelerate the MoM by discretizing integral equations with the CBF, which in general has smaller DOFs than the RWG functions. For generating the CBF, the boundary of a scatterer is divided into N^{Cell} cells. The nth CBF in cell m, denoted by $\mathbf{c}_{mn}$, is represented as the linear combination of the RWG function:

$$\mathbf{c}_{mn}(\boldsymbol{r}) = \sum_{i=1}^{N_m} c_{mni}\boldsymbol{f}_{\Lambda_{mi}}(\boldsymbol{r}) \quad (n = 1, \cdots L_m), \quad (11)$$

where N_m and Λ_{mi} are the total number and index of the RWG function in cell m, and c_{mni} are complex coefficients. The complex matrix $\mathbf{C}_m \in \mathbb{C}^{N_m \times N_m^{\mathrm{CBF}}}$ consisting of the coefficients c_{mni}:

$$\left[\mathbf{C}_m\right]_{in} = c_{mni}. \quad (12)$$

is also referred to as the CBF in cell m in this paper.

One of widely used methods to generate the CBF is as follows. Considering scattering problems whose scatterer is a part of the original one included in cell m, one computes the solution of the problem with multiple incident plane waves from s directions as wave sources. We define the solution in cell m with the ith incident wave as $\mathbf{j}_{m,i}$ and $\mathbf{J}_m$ by

$$\mathbf{J}_m = \begin{bmatrix}\mathbf{j}_{m,1} & \mathbf{j}_{m,2} & \cdots & \mathbf{j}_{m,s}\end{bmatrix}. \quad (13)$$

Once the coefficient matrix $\mathbf{J}_m$ is calculated, the conventional CBFM computes the CBF $\mathbf{C}_m$ by algebraically orthogonalizing $\mathbf{J}_m$ with the singular value decomposition (SVD):

$$\begin{aligned}\mathbf{J}_m &= \mathbf{U}\mathbf{\Sigma}\mathbf{V}^H \\ &= \begin{bmatrix}\mathbf{U}_{\mathrm{L}} & \mathbf{U}_{\mathrm{S}}\end{bmatrix}\begin{bmatrix}\mathbf{\Sigma}_{\mathrm{L}} & \\ & \mathbf{\Sigma}_{\mathrm{S}}\end{bmatrix}\begin{bmatrix}\mathbf{V}_{\mathrm{L}}^H \\ \mathbf{V}_{\mathrm{S}}^H\end{bmatrix} \\ &\simeq \mathbf{U}_{\mathrm{L}}\mathbf{\Sigma}_{\mathrm{L}}\mathbf{V}_{\mathrm{L}}^H, \end{aligned} \quad (14)$$

where $\mathbf{U} \in \mathbb{C}^{N_m \times r}$ and $\mathbf{V} \in \mathbb{C}^{s \times r}$ are unitary matrices and $\mathbf{\Sigma} \in \mathbb{C}^{r \times r}$ is the diagonal matrix having r singular values in its diagonal components. Here, Σ is split into two matrices Σ_L and Σ_S with the use of a threshold δ_{SVD}, namely Σ_L is the diagonal matrix with the singular values of $\mathbf{J}_m$ larger than $\sigma_1\delta_{\mathrm{SVD}}$ while Σ_S is the one with smaller singular values, where σ_1 is the largest singular value of $\mathbf{J}_m$. The submatrix of $\mathbf{U}$ corresponding to $\mathbf{\Sigma}_{\mathrm{L}}$, denoted by $\mathbf{U}_{\mathrm{L}} \in \mathbb{C}^{N_m \times N_m^{\mathrm{CBF}}}$, is used as the CBF $\mathbf{C}_m$. The CBF $\mathbf{C}_m$ obviously satisfies $\mathbf{C}_m^H\mathbf{C}_m = I$, which means that the coefficient vectors of the CBFs in each cell are algebraically orthogonalized.

3.2. Proposed Algorithm

The CBFs are created from the excitation current of each cell. One of the simplest methods to generate CBF is to compute $\mathbf{j}_{m,i}$ as solutions of scattering problems in cell m without taking into account the mutual couplings between cells, namely

$$\mathbf{j}_{m,i} = \mathbf{Z}_{mm}^{-1}(\mathbf{v}_i)_m, \quad (15)$$

where $\mathbf{Z}_{mm} \in \mathbb{C}^{N_m \times N_m}$ is submatrix of the impedance matrix $\mathbf{Z}$ formed by N_m RWG functions in cell m and $(\mathbf{v}_i)_m \in \mathbb{C}^{N_m}$ is the subvector of the ith incident field vector $\mathbf{v}_i$ for cell m [10]. For $\mathbf{v}_i$, the plane waves propagating in the directions sampled at an appropriate interval from the three-dimensional unit sphere are used. The CBF generated from $\mathbf{j}_{m,i}$ in (15) is called the primary CBF [11]. In addition to the primary CBFs, several types of CBFs exist, such as secondary CBFs generated from the current of other cells [10] and higher-order CBFs [17]. In Tanaka et al. [15,16], we have proposed IPCBFs, which iteratively include the effect of the higher-order CBFs into the primary CBF without increasing the number of basis functions. The expansion coefficient vector $\mathbf{j}_{m,i}^{(p)}$ with p iterations for the IPCBF is obtained by

$$\mathbf{j}_{m,i}^{(p)} = \mathbf{Z}_{mm}^{-1}\left((\mathbf{v}_i)_m - \sum_{\substack{n=1 \\ n\neq m}}^{N^{\mathrm{Cell}}} \mathbf{Z}_{mn}\mathbf{j}_{n,i}^{(p-1)}\right). \quad (16)$$

This method not only prevents the number of CBFs from increasing, but also efficiently add the effects of the higher-order CBFs to the primary CBFs. Note that equation (16) can be interpreted as the solution of the MoM with p iterations of the block Jacobi method. According to this idea, we have further developed a numerical method to obtain IPCBF with the rough use of the Krylov subspace algorithm to (8)

instead of (16) [19]. In our previous study [19], we have used the block BiCGStab [20,21] for generating the IPCBF. In fact the block BiCGStab seems appropriate for this purpose since it can simultaneously solve linear systems with multiple incident waves by generating the Krylov subspace from the initial residuals based on the incident plane waves with s directions. However the block-type Krylov subspace method is not as effective as was expected since the initial residuals calculated from plane waves with multiple directions are in general almost linearly dependent and thus the dimension of the Krylov subspace is less than the number of the basis functions. By this reason, we utilize the standard generalized minimal residual (GMRES) method [22] as the Krylov subspace algorithm in this paper. Hence $\mathbf{j}_{m,i}^{(p)}$ is computed one by one for each RHS $\mathbf{v}_i$.

One of issues of the IPCBF is a trade-off between accuracy and computational cost. When the interval of the incident waves for calculating the IPCBF is too wide, we cannot calculate RCS patterns accurately even if the IPCBFs are generated from sufficiently converged iterative solutions obtained with GMRES. On the other hand, it is desirable to use smaller numbers of incident wave sources in order to reduce the computational cost of IPCBF. We therefore propose a hybrid algorithm of using CBFM and the original matrix equation in (8) together as a way to obtain a solution with better accuracy while using these IPCBFs. This algorithm utilizes the feature that one may roughly capture the characteristics of RCS using these IPCBFs.

In this algorithm, the IPCBF is first computed with sparsely sampled incident wave sources and relatively large residual norm. The IPCBF is then used to calculate the unknown current, denoted by $\mathbf{j}^{(0)}$, with CBFM. The current $\mathbf{j}^{(0)}$ is used as the initial value for the iteration in the MoM since $\mathbf{j}^{(0)}$ is expected to broadly capture the characteristics of the correct current $\mathbf{j}$. From a different point of view, one may say that this algorithm tries to reduce the number of iterations of the conventional MoM by improving the initial value with the help of CBFM.

Algorithm 1 shows the proposed hybrid algorithm which consists of three procedures. The first procedure is for the generation of $\mathbf{C}_m$ for the IPCBFs. The loop for $i = 1$ to s is the calculation scheme for the IPCBF $\mathbf{J}_m$. In the next loop for $m = 1$ to N^{Cell}, $\mathbf{J}_m$ is algebraically orthogonalized and compressed by the SVD. The second procedure is for preparing a matrix for the CBFM with the LU decomposition, which is more effective for this procedure than iterative methods since the LU decomposition can efficiently obtain solutions for linear equations with a small coefficient matrix and multiple sources. The third procedure is the final iteration scheme for obtaining the current $\boldsymbol{J}(\boldsymbol{r})$. We first calculate $\mathbf{j}^{\mathrm{CBF}}$, which is the solution of the discretized CFIE:

Algorithm 1 Hybrid Algorithm using CBFM and MoM

procedure Coefficient Generation
  for $i = 1, \cdots, s$ **do**
    Set $\mathbf{v}$ for direction i from (10)
    Solve $\mathbf{Z}\mathbf{j}_i = \mathbf{v}$ in (8) for $\mathbf{j}_i$ with a tolerance δ_{r}.
    for $m = 1, \cdots, N^{\mathrm{Cell}}$ **do**
      Divide $\mathbf{j}_i$ into elements per cell $\mathbf{j}_{m,i}$
    end for
  end for
  for $m = 1, \cdots, N^{\mathrm{Cell}}$ **do**
    Orthogonalize $\mathbf{J}_m \simeq \mathbf{U}_{\mathrm{L}}\mathbf{\Sigma}_{\mathrm{L}}\mathbf{V}_{\mathrm{L}}^H$ by (14)
    Assign $\mathbf{U}_{\mathrm{L}}$ to $\mathbf{C}_m$
  end for
end procedure

procedure CBFM Matrix Filling
  Compute $\mathbf{Z}^{\mathrm{CBF}}$ in (18)
  Decompose $\mathbf{Z}^{\mathrm{CBF}}$ by using LU decomposition
end procedure

procedure Final Iteration
  for $i = 1, \cdots, S$ **do**
    Set $\mathbf{v}^{\mathrm{CBF}}$ for direction i from (19)
    Solve $\mathbf{Z}^{\mathrm{CBF}}\mathbf{j}^{\mathrm{CBF}} = \mathbf{v}^{\mathrm{CBF}}$ in (17) for $\mathbf{j}^{\mathrm{CBF}}$
    Compute $\mathbf{j}^{(0)}$ and set it as initial value
    Solve $\mathbf{Z}\mathbf{j} = \mathbf{v}$ in (8) for $\mathbf{j}$ with a tolerance δ_{R}.
    Compute current $\boldsymbol{J}(\boldsymbol{r})$ from (7)
  end for
end procedure

$$\mathbf{Z}^{\mathrm{CBF}}\mathbf{j}^{\mathrm{CBF}} = \mathbf{v}^{\mathrm{CBF}} \tag{17}$$

with the IPCBF, where

$$\mathbf{Z}^{\mathrm{CBF}} = \mathbf{C}^H\mathbf{Z}\mathbf{C}, \tag{18}$$

$$\mathbf{v}^{\mathrm{CBF}} = \mathbf{C}^H\mathbf{v}, \tag{19}$$

$$\mathbf{C} \equiv \begin{bmatrix} \mathbf{C}_1 & & \\ & \ddots & \\ & & \mathbf{C}_{N^{\mathrm{Cell}}} \end{bmatrix}. \tag{20}$$

Then we apply the GMRES to the CFIE discretized with the RWG functions with $\mathbf{j}^{(0)} = \mathbf{C}\mathbf{j}^{\mathrm{CBF}}$ as the initial guess.

The advantage of the proposed method is that it can always converge to within an arbitrary accuracy, even if the solution of CBFM with IPCBF is not accurate. If the accuracy of IPCBF is sufficient, the final iteration scheme is not performed and the solution is obtained. In other words, the proposed method can seamlessly select cases where the accuracy of CBFM is sufficient, and can control the analysis accuracy. In addition, IPCBFs do not require extended regions which are used in the conventional CBFM in order to avoid unnatural behavior of the solution near the boundaries of cells [10]. Furthermore, for the Krylov subspace algorithm, the computation can be made more efficient with the help of FMM [6, 7], which would further speed up the IPCBF generation.

An advantage of the proposed method from the viewpoint of program implementation is that it can use the matrix solving procedure in the conventional MoM code for calculating $\mathbf{C}_m$ and for the final iteration in the hybrid algorithm. There is obviously no complication in the process caused by the extended region. In addition, the advantage of the CBFM implementation that the matrix equation of the CBFM is generated simply by taking the inner product of the coefficient $\mathbf{C}_m$ and $(\mathbf{Z}, \mathbf{v})$ remains unchanged. Therefore, one can easily implement the proposed method using any existing in-house MoM program.

4. Numerical Results

In this section, we show numerical examples with two types of perfect electric conductor scatterers, a plate and an almond. Hereafter the CBFM using the IPCBFs will be referred to as "IPCBFM" in order to distinguish it from the proposed hybrid algorithm. The residual norms of (8) solved in the procedure of the coefficient generation and the final iteration in Algorithm 1 are denoted by δ_{r} and δ_{R}, respectively. The GMRES method and FMM are used in the above procedure. The calculation by the standard MoM is also performed for the comparison with these methods. We use the RCS, denoted by σ, as the evaluation index of the spatial distribution of scattering in the far field. The RCS σ for the current excited by the incident plane wave $\boldsymbol{E}^{\mathrm{inc}}(\boldsymbol{r})$ is expressed as follows:

$$\sigma = \lim_{r\to\infty} 4\pi r^2 \frac{\left|\boldsymbol{E}^{\mathrm{scat}}(\boldsymbol{r})\right|^2}{\left|\boldsymbol{E}^{\mathrm{inc}}(\boldsymbol{r})\right|^2}, \tag{21}$$

where $\boldsymbol{E}^{\mathrm{scat}}(\boldsymbol{r}) = \eta(\mathcal{T}'\boldsymbol{J})(\boldsymbol{r})$ is the scattered field.

4.1. Plate

We calculate the RCS pattern of the plate shown in the Fig. 2 and evaluate its analysis accuracy and convergence. The number of the unknowns N in the MoM is 22050. Analysis coordinate plane (the coordinate plane on which σ is calculated) is $z-x$ plane ($\phi = 0^\circ$ plane). We calculate the

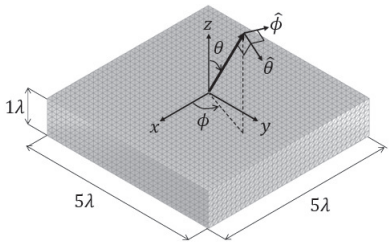

Fig. 2: Plate

RCS pattern of $0^\circ \le \theta \le 90^\circ$, $\Delta\theta = 1^\circ$ of $\hat{\theta}$ polarization; therefore, the number of the incidence S is equal to 91. The scatterer is divided into 4, 4, and 2 cells in the x, y, and z directions, respectively. The longest side length of the cell l^{Cell} is 1.25λ and the total number of cells N^{Cell} is 32. We set the coefficient γ of CFIE in (6) as 2.0×10^{-1}. The typical threshold value δ_{SVD} is usually around 10^{-3} [11]. If the threshold is too large, one may lose necessary CBFs, which makes it difficult to evaluate the characteristics of IPCBFM. To prevent this, we use a smaller value 10^{-7} for δ_{SVD} in this paper. In this analysis, we set the tolerance of the residual norm δ_{R} to be 10^{-4} at the final iteration in the hybrid algorithm and the MoM.

TABLE 1 shows the calculation parameters for generating the CBFs. For conditions 1 to 4, the CBFs are generated by sampling the incident plane wave from the coordinate plane and range in which the RCS is finally computed, and the angular intervals and the residual norms δ_{r} are varied. The polarization of condition 1–4, 6, 7 is $\hat{\theta}$ and that of condition 5 is $\hat{\phi}$. The conditions 6 and 7 have the same number of the incident waves s as in condition 1, but the coordinate planes to be sampled are different from in other conditions. We analyze the effects of the residual norm δ_{r}, the angle interval $\Delta\theta$, the polarization, and the coordinate plane selection on CBF generation and analysis accuracy through these analyses.

Table 1: Parameters for the CBF generations

Condition	θ_{s}	ϕ_{s}	$\Delta\theta$	$\Delta\phi$	N_θ	N_ϕ	N_{p}(Pol.)	δ_{r}
1	0°	0°	10°	0°	10	1	1 ($\hat{\theta}$)	10^{-4}
2	0°	0°	10°	0°	10	1	1 ($\hat{\theta}$)	10^{-2}
3	0°	0°	30°	0°	4	1	1 ($\hat{\theta}$)	10^{-4}
4	0°	0°	30°	0°	4	1	1 ($\hat{\theta}$)	10^{-2}
5	0°	0°	10°	0°	10	1	1 ($\hat{\phi}$)	10^{-4}
6	0°	90°	10°	0°	10	1	1 ($\hat{\theta}$)	10^{-4}
7	90°	0°	0°	10°	1	10	1 ($\hat{\theta}$)	10^{-4}

Fig. 3 shows the number of the CBFs N^{CBF}, the total number of the iterations for the CBF generations T^{CBF} and that for the final iterations T^{Final}. In the hybrid algorithm, if N^{CBF} is small enough, the computational complexity of the SVD ($O\left(s^2 N_m\right)$) and the LU decomposition ($O\left(\left(N^{\mathrm{CBF}}\right)^3\right)$)

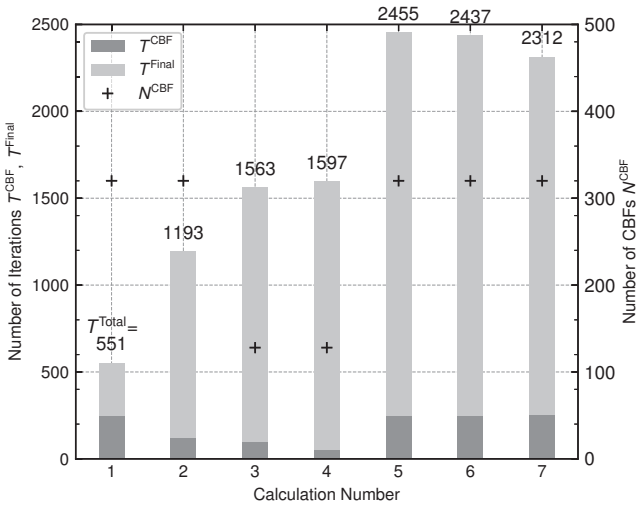

Fig. 3: Iteration results for the plate

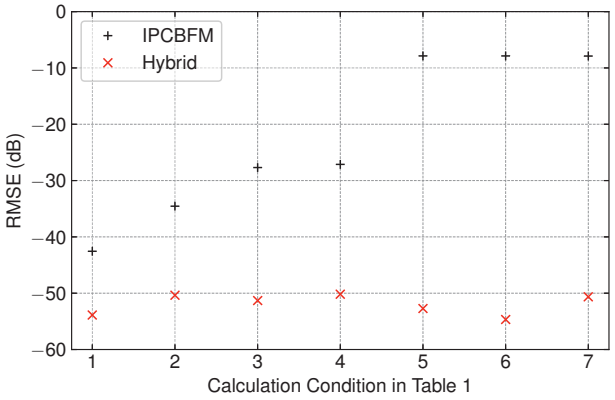

Fig. 4: RMSE of the plate

become much smaller than that of the IPCBF generation and the final iterations. Therefore, the overall computational complexity of the hybrid algorithm will be approximately proportional to the number of these iterations. We thus define the total number of iterations in an analysis as $T^{\mathrm{Total}}(= T^{\mathrm{CBF}} + T^{\mathrm{Final}})$. We note that the number of the iterations for the MoM T^{MoM} is 2122. We also note that N^{CBF} is small enough that the matrix equation shown in (17) can be calculated by LU decomposition.

Fig. 4 shows the root mean square error (RMSE) for each of conditions in TABLE 1. The RMSE of the CBFM relative to the MoM is defined by

$$\mathrm{RMSE} = 10 \log 10 \left(\frac{\sqrt{\frac{1}{N_\theta} \sum_{i=1}^{N_\theta} (\sigma_i^{\mathrm{c}} - \sigma_i^{\mathrm{m}})^2}}{\max_i\{\sigma_i^{\mathrm{m}}\} - \min_i\{\sigma_i^{\mathrm{m}}\}} \right) \quad \mathrm{dB},$$

where σ_i^{m} (σ_i^{c}) stands for σ computed with MoM (CBFM) for the ith incident wave. In Fig. 4, the RMSE for the result of the IPCBFM under the condition 1 in TABLE 1 is better than that under the condition 2. It indicates that using a current distribution close to the correct solution for the CBF generation improves the accuracy of the CBFM analysis. As

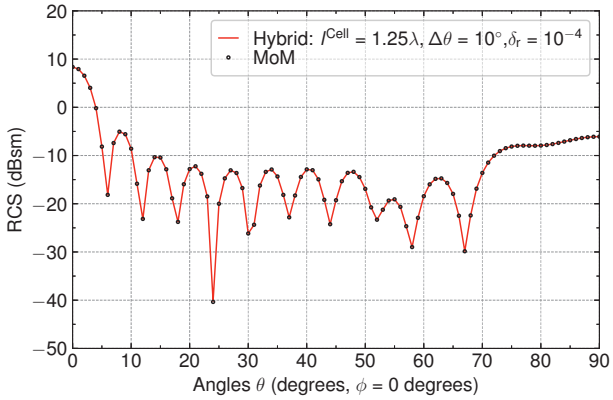

Fig. 5: RCS of the plate

can be seen from the RMSEs for the IPCBFM results under the condition 3 and 4, this will not be the case if the number of CBFs is not sufficient to represent the distribution of induced currents for each direction of the RCS pattern. When the CBFs are generated from the incident plane waves with the orthogonal polarization ($\hat{\phi}$ polarization) in calculation number 5, the RMSE of the IPCBFM becomes over -10 dB. This is also the case when the plane wave is sampled from the coordinate planes ($y - z$ and the $x - y$) different from the plane where the RCS pattern is to be obtained ($z - x$) (i.e., conditions 6 and 7).

One can simply conclude from these results that more incident wave samples are needed to further improve the accuracy of the analysis. On the other hand, as the number of samples is increased, the acceleration effect of the CBFM to the ordinary MoM decreases. The number of sampling points is also largely dependent on the scatterer. As shown in Fig. 4, the hybrid algorithm solves this problem. In the present analysis, the hybrid algorithm yields a solution with RMSE below -50 dB, which agrees very well with the MoM results. The total number of iterations for the calculation number 5 to 7 in the hybrid algorithm exceeds that of MoM. It means that the hybrid algorithm is not effective unless the initial values are reasonable. On the other hand, if good initial values are chosen, the hybrid algorithm can speed up the process. In the case of calculation number 1, which meets this condition, the total number of iterations is reduced by a factor of about 1/4.

The RCS patterns of calculation number 1 for the hybrid method, which showed particularly high efficiency in this analysis, are shown in Fig. 5. The analysis results agree well with the results of the MoM.

4.2. Almond

In this section, we investigate the parameter dependency of the proposed method by analyzing the almond-shaped scatterer [23] in Fig. 6 whose longest length is 10λ. The

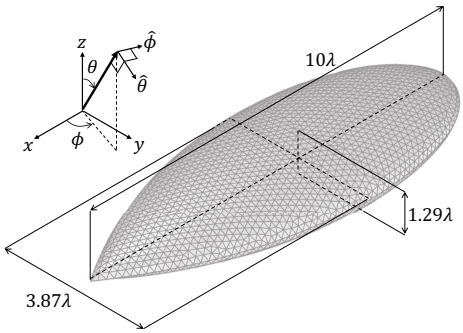

Fig. 6: Almond

number of the unknowns N is 8244. We calculate the RCS pattern of $-90^\circ \leq \theta \leq 90^\circ$, $\Delta\theta = 0.5^\circ$ of θ polarization ($S = 361$). TABLE 2 shows the parameters for the IPCBF generation. In this calculation, we use two types of the CBFs, the IPCBFs and the primary CBFs, and compare the differences between them. We consider two types of the cells: $l^{\mathrm{Cell}} = 1.25\lambda$ and 2.5λ per side. The scatterer is divided into $8 \times 4 \times 2$ cells for $l^{\mathrm{Cell}} = 1.25\lambda$ and $4 \times 2 \times 2$ cells for $l^{\mathrm{Cell}} = 2.5\lambda$ for the x, y, z directions; hence the number of the cells containing the RWGs excluding empty cells are $N^{\mathrm{Cell}} = 60$ and 16, respectively. Then, three intervals of incident angles $\Delta\theta = 2.5^\circ$, 5°, and 10° are considered. The angular range, the polarization, and the sampling coordinate plane are the same as those for the RCS pattern in the final solutions. The residual norm δ_{r} for the IPCBF generation is set as 10^{-4} or 10^{-2}. The currents to generate the primary CBFs is calculated in each cell with the LU decomposition. We consider all combinations of these parameters. The residual norm δ_{R} for final iteration and the MoM is set to 10^{-6}.

Table 2: Parameters for the IPCBF generations

Parameter	Value
Cell Size l^{Cell} (N^{Cell})	1.25λ (60), 2.5λ (16)
Interval $\Delta\theta$ ($N_\theta = s$)	10° (19), 5° (37), 2.5° (73)
Polarization	$\hat{\theta}$
Residual Norm δ_{r}	10^{-4}, 10^{-2}
SVD Threshold δ_{SVD}	10^{-7}

The numbers of the CBFs N^{CBF} are shown in Fig. 7. Note that N^{CBF}/N is less than one half. Smaller values of the sampling points tend to have fewer N^{CBF} for the IPCBFs. On the other hand, N^{CBF} for the primary CBFs remained almost unchanged even though the number of the sampling points increases. It depends only on the cell size in the case of primary CBFs. This is because the primary CBFs are made from the current of only one cell. In the generation of primary CBFs, there is no significant difference in the current excited in one small cell even if the incident angle is changed slightly in the same coordinate plane. This means that increasing the number of incident wave samples does not lead to an increase in information. When the incident coordinate plane is not limited to that for calculating the RCS, the primary CBF could be sufficiently rich to represent the complex current [11]. However, this results in creating many extra CBFs even though we only want to obtain the RCS for a specific coordinate plane. On the other hand, the IPCBFs are also CBFs generated for each cell, but their original currents are obtained from calculations for the entire region. Hence the IPCBFs are subject to the effect of currents that vary in a complicated way depending on the direction of the incident wave in a specific coordinate plane. Therefore the IPCBFs can generate many independent CBFs with incident waves on a specific coordinate plane. Also it can be seen in Fig. 7 that δ_{r} has almost no effect on the number of CBFs for the same cell size.

Fig. 8 shows the the RMSE for the IPCBFM and hybrid method, and ratio of T^{Total} to $T^{\mathrm{MoM}}(= 11110)$ for the hybrid method. In Fig. 8a, it can be seen that accuracy of the IPCBFM highly depends on the number of the sampling points. On the other hand, no matter what the initial value is, the RMSE will eventually be less than -60 dB in the hybrid method as shown in Fig. 8b. In other words, the hybrid method allows IPCBFM analysis results to be controlled to any desired level of accuracy. This is also valid when primary CBF is used as CBF. However, since the primary CBF does not give a good initial value, the number of iterations when the hybrid method is used is only 0.9 times the number of iterations when it is not used as shown in Fig. 8c. On the other hand, when combined with IPCBF, the computation becomes up to 5 times faster. These results indicate that the hybrid method is particularly effective when combined with IPCBF. Fig. 9 shows the RCS pattern of the MoM and the hybrid method under the condition of $l^{\mathrm{Cell}} = 1.25\lambda$ and $\delta_{\mathrm{r}} = 10^{-4}$. The results obtained by the proposed method agree well with the MoM results overall. From these results, it can be said that the proposed method is a fast method to obtain RCS patterns in a specific coordinate plane with arbitrary accuracy.

5. Conclusion

For reducing the number of iterations and unknowns in the MoM, we proposed a hybrid algorithm combining the CBFM and the MoM by using IPCBFs. The proposed methods are formulated, and verified numerically as we analyze the RCS of two scatterers. By using proposed methods, we could obtain solutions with good accuracy and faster than with conventional method. In this study, we conducted numerical analyses without any preconditioning for the iterative method in order to purely verify the performance of the

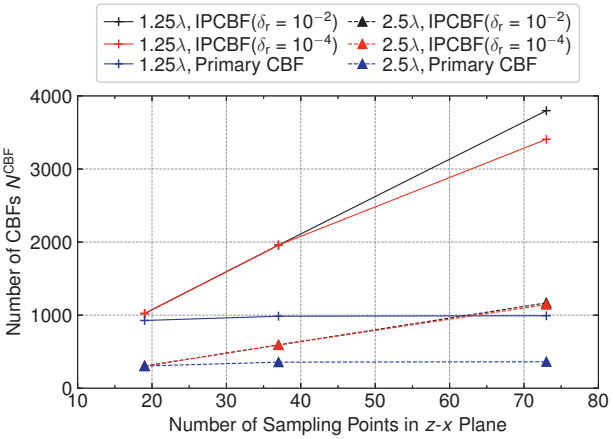

Fig. 7: Number of CBFs N^{CBF}

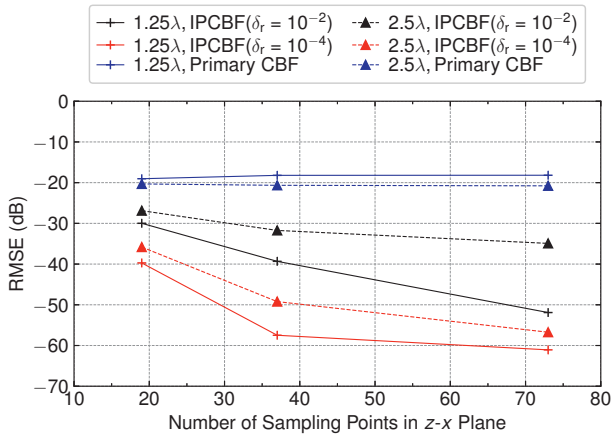

(a) RMSE (IPCBFM)

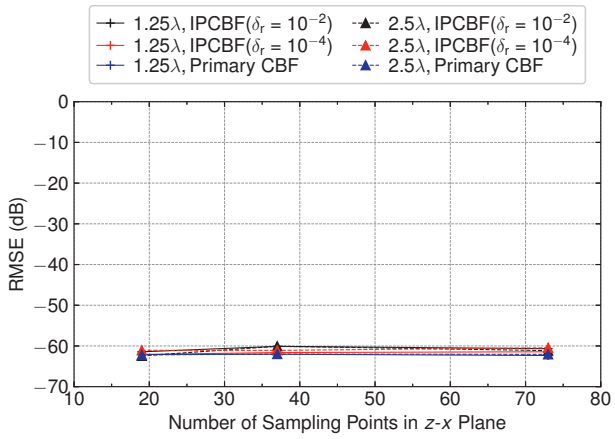

(b) RMSE (hybrid method)

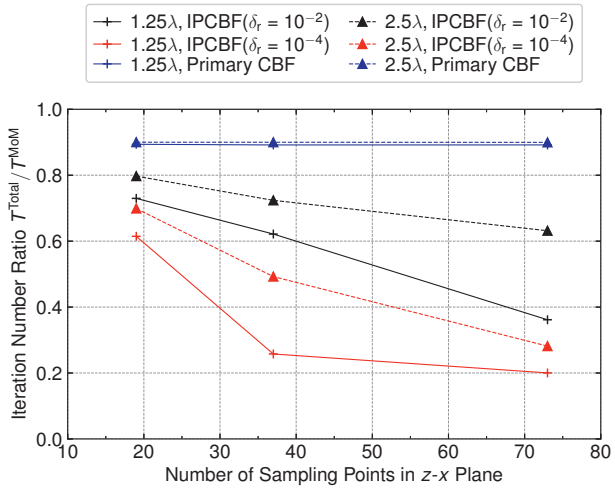

(c) Iteration number ratio of $T^{\mathrm{Total}}/T^{\mathrm{MoM}}$

Fig. 8: Analysis result of the almond by using the IPCBFM and the hybrid method

proposed methods. We believe that preconditioning methods can be easily incorporated into the proposed method, and the matrix generation and final iteration time will be even faster. Furthermore, we realize that the validity of the IPCBF for other integral equations than CFIE will need to be verified. In particular, we plan to extend the ideas of the IPCBF in the present formulation to the analysis of dielectrics.

References

(1) E. F. Knott, J. F. Shaeffer, and M. T. Tuley, *Radar Cross Section*, 2nd ed. Boston, USA: Artech House, 1993.

(2) R. G. Kouyoumjian and P. H. Pathak, "A uniform geometrical theory of diffraction for an edge in a perfectly conducting surface," *IEEE Trans. Antennas Propag.*, vol. 62, no. 11, pp. 1448–1461, Nov. 1974.

(3) J.-M. Jin, *The Finite Element Method in Electromagnetics*, 3rd ed. New York: Wiley-IEEE Press, 2014.

(4) A. Taflove and S. C. Hagness, *Computational Electrodynamics: The Finite-Difference Time-Domain Method*, 3rd ed. Boston: Artech House, 2005.

(5) R. F. Harrington, *Field Computation by Moment Methods*. Piscataway, NJ: IEEE Press, 1993.

(6) J. Song, C.-C. Lu, and W. C. Chew, "Multilevel fast multipole algorithm for electromagnetic scattering by large complex objects," *IEEE Trans. Antennas Propag.*, vol. 45, no. 10, pp. 1488–1493, Oct. 1997.

(7) O. Ergül and L. Gürel, *The Multilevel Fast Multipole Algorithm (MLFMA) for Solving Large-Scale Computational Electromagnetics Problems*. New York, USA: Wiley-IEEE Press, 2014.

(8) A. Heldrig, J. M. Rius, J. M. Tamayo, J. Parrón, and E. Úbeda, "Fast direct solution of method of moments linear system," *IEEE Trans. Antennas Propag.*, vol. 55, no. 11, pp. 3220–3228, Nov. 2007.

(9) R. Gholami, J. Mojolagbe, A. Menshov, F. S. H. Lori, and V. Okhmatovski, "$\mathcal{H}$-matrix arithmetic for fast

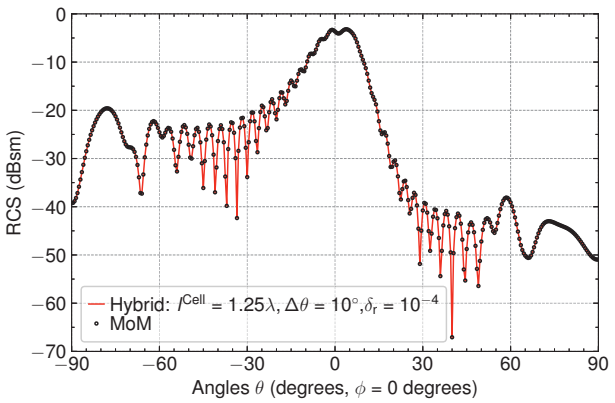

Fig. 9: RCS pattern of the almond

direct and iterative method of moment solution of surface-volume-surface EFIE for 3-D radiation problems," *Progress In Electromagnetics Research B*, vol. 82, pp. 189–210, Dec. 2018.

(10) V. V. S. Prakash and R. Mittra, "Characteristic basis function method: a new technique for efficient solution of method of moments matrix equations," *Microw. Opt. Techn. Let.*, vol. 36, no. 2, pp. 95–100, Jan. 2003.

(11) E. Lucente, A. Monorchio, and R. Mittra, "An iteration-free MoM approach based on excitation independent characteristic basis functions for solving large multiscale electromagnetic scattering problems," *IEEE Trans. Antennas Propag.*, vol. 56, no. 4, pp. 999–1007, Apr. 2008.

(12) R. Mittra and K. Du, "Characteristic basis function method for iteration-free solution of large method of moments problems," *Progress In Electromagnetics Research B*, vol. 6, pp. 307–336, May 2008.

(13) R. Maaskant, R. Mittra, and A. G.Tijhuis, "Fast analysis of large antennas arrays using the characteristic basis function method and the adaptive cross approximation algorithm," *IEEE Trans. Antennas Propag.*, vol. 56, no. 11, pp. 3440–3451, Nov. 2008.

(14) S. Rao, D. Wilton, and A. Glisson, "Electromagnetics scattering by surfaces of arbitrary shape," *IEEE Trans. Antennas Propag.*, vol. 30, no. 3, pp. 409–418, May 1982.

(15) T. Tanaka, Y. Inasawa, Y. Nishioka, and H. Miyashita, "Improved primary characteristic basis function method for monostatic radar cross section of specific coordinate plane," *IEICE Trans. Electron.*, vol. E99-C, no. 1, pp. 28–35, Jan. 2016.

(16) T. Tanaka, Y. Inasawa, Y. Nishioka, and H. Miyashita, "Improved primary characteristic basis function method considering higher-order multiple scattering," *IEICE Trans. Electron.*, vol. E100-C, no. 1, pp. 45–51, Jan. 2017.

(17) S. G. Hay, J. D. O'Sullivan, and R. Mittra, "Connected patch array analysis using the characteristic basis function method," *IEEE Trans. Antennas Propag.*, vol. 59, no. 6, pp. 1828–1837, Jun. 2011.

(18) J. Nédélec, *Acoustic and Electromagnetic Equations: Integral Representations for Harmonic Problems.* New York: Springer-Verlag, 2001.

(19) T. Tanaka, K. Niino, N. Nishimura, M. Takikawa, and N. Yoneda, "A generation scheme of the characteristic basis functions by using block Krylov subspace algorithm (Japanese)," *Trans. Jpn. Soc. Comput. Methods Eng.*, vol. 19, pp. 99–102, Dec. 2019.

(20) A. E. Guennouni, K. Jbilou, and H. Sadok, "A block version of BiCGSTAB for linear systems with multiple right-hand sides," *Elec. Trans. Numer. Anal.*, vol. 16, pp. 129–142, Jan. 2003.

(21) Y. Nakamura, K.-I. Ishikawa, Y. Kuramashi, T. Sakurai, and H. Tadano, "Modified block BiCGSTAB for lattice QCD," *Comput. Phys. Commun.*, vol. 183, pp. 34–37, Jan. 2012.

(22) Y. Saad, *Iterative Methods for Sparse Linear Systems.* PA, USA: SIAM, 2003.

(23) A. C. Woo, H. T. G. Wang, M. J. Schuh, and M. L. Sanders, "EM programmer's notebook-benchmark radar targets for the validation of computational electromagnetics programs," *IEEE Trans. Antennas Propag.*, vol. 35, no. 1, pp. 84–89, Feb. 1993.